Performance Analysis of IoT Networks with UAV-assisted NOMA-based WPT-MEC

ANH-NHAT NGUYEN*, DINH-CUONG HOANG, GIA-HUY NGUYEN, and TIEN-DUNG DO, FPT University, Hanoi, Vietnam

This paper investigates the performance of an Internet of Things (IoT) system utilizing a unmanned aerial vehicle (UAV) in an urban environment with the assistance of non-orthogonal multiple access (NOMA) based mobile-edge computing (MEC). We consider two clusters of IoT device (ID) with limited resources that can harvest energy from a power beacon (PB) in order to offload their tasks to a UAV. We propose a four-phase protocol for energy harvesting (EH) and offloading task of IDs. To evaluate offloading performance, we derive the expression of successful computation probability (SCP) for the whole system. In addition, we present a formulation of the optimization problem that optimizes the SCP by optimizing the EH time and height of the UAV. The issue was resolved using particle swarm optimization (PSO). On the basis of the Monte Carlo simulation, a number of system parameters, including the number of IDs in each cluster, the EH time, and the height of the UAV, are evaluated to verify the accuracy of our analysis.

Additional Key Words and Phrases: internet of things, unmanned aerial vehicles, energy harvesting, wireless power transfer, mobile edge computing, nonorthogonal multiple access, particle swarm optimization

ACM Reference Format:
Anh-Nhat Nguyen, Dinh-Cuong Hoang, Gia-Huy Nguyen, and Tien-Dung Do. 2023. Performance Analysis of IoT Networks with UAV-assisted NOMA-based WPT-MEC. 1, 1 (November 2023), 10 pages. https://doi.org/10.1145/nnnnnnn.nnnnnnn

1 INTRODUCTION

Over the years, technical innovation has displayed great results in a variety of fields, most notably in the Internet of Things (IoT), where considerable steps have been achieved in the development of intelligent sensory gear such as smart vehicles, devices, and cites [1]. Nevertheless, IoT networks face challenges related to signal propagation over long distances and efficient data transmission from IoT devices (IDs). Additionally, the constrained battery lifespan and computational limitations inherent to these IDs present intricate and demanding hurdles to overcome [6].

To tackle these aforementioned challenges, two promising strategies have come to the forefront: wireless power transfer (WPT) and mobile-edge computing (MEC), which offer potential solutions for enhancing computational tasks and device energy. Using the powerful computing capabilities of MEC, IDs can easily send some or all of their processing tasks to servers strategically placed at the edges of networks [13]. An additional concern pertains to the limited operational lifespan of ID batteries. As a result, WPT is a possible choice for resolving this issue. By using radio frequency

*The author was the main contributor to this research.

Authors' address: Anh-Nhat Nguyen, nhatna3@fe.edu.vn; Dinh-Cuong Hoang, cuonghd7@fe.edu.vn; Gia-Huy Nguyen, huynghe180064@fpt.edu.vn; Tien-Dung Do, dungdthe170502@fpt.edu.vn, FPT University, Hanoi, Vietnam, 10000.

XXXX-XXXX/2023/11-ART $15.00
https://doi.org/10.1145/nnnnnnn.nnnnnnn

(RF) energy harvesting (EH), IDs can get power from outside sources, which increases the amount of time these devices can run on batteries[9].

Nonetheless, the IoT architecture's stationary framework has a limited transmission range and may experience signal attenuation among its components. Unmanned aerial vehicles (UAVs) are a viable option for fortifying the infrastructure and aiding IDs in information dissemination due to their exceptional agility and cost-effective operation [8, 9]. Moreover, IDs offload their computational burden onto a UAV server that is seamlessly integrated with a MEC server, thereby enhancing processing efficiency while simultaneously decreasing communication latency. In addition, WPT facilitates the UAV's function as a mobile power hub for terrestrial users, thus improving the energy efficiency of IDs [7, 14].

Moreover, the utilization of non-orthogonal multiple access (NOMA) facilitates the concurrent access of a substantial multitude of IDs to both IoT networks and radio frequency assets, achieved through the exploitation of diverse power strata. To elaborate, NOMA's merits encompass the facilitation of exceedingly voluminous data transmission and the augmentation of spectral efficiency, distinguishing it from alternative wireless paradigms such as orthogonal multiple access (OMA) [11]. When NOMA is combined with the UAV-enabled MEC framework, both the IoT network's ability to send data and to do computations are made better [5].

Inspired by the preceding discourse, this study delves into the realm of UAV-assisted NOMA within the context of MEC, where the UAV act as aerial computing support station. Our investigation contemplates the scenario wherein IDs harness RF EH from the power beacon (PB) for the purpose of task offloading. Moreover, an assessment is conducted pertaining to the likelihood of Line-of-Sight (LoS) and Non Line-of-Sight (NLoS) conditions governing wireless communication between the UAV and IDs under Rayleigh fading channel. The following are the primary contributions of our paper:

- We investigated a system including a UAV-assisted NOMA-based WPT-MEC in IoT networks with IDs that can harvest energy from a PB. In addition, we proposed a system protocol that would guarantee an effective EH and offload tasks.
- We derived a SCP closed-form expression for the whole system. Furthermore, we proposed a problem to maximize the SCP through the optimization of both the EH time of IDs and the height of UAV. The issue was resolved with a PSO algorithm.
- In order to validate the effectiveness of our system, numerical results are employed to assess the offloading performance of the system. These metrics include the transmit power of the PB, the number of IDs in two clusters, the EH time of ID, and height of UAV.

The rest of this paper is organized as follows. In Section 2, the system model and the time-switching protocol are introduced. In Section 3, the SCP is analyzed, and optimization for maximum SCP is also provided. In Section 4, numerical results are presented and discussed. Finally, conclusions are presented in Section 5.

2 SYSTEM MODEL AND COMMUNICATION PROTOCOL

2.1 System and channel model

In Fig. 1, we consider a UAV-assisted NOMA-based WPT-MEC in IoT networks with two limited resources ID clusters: cluster A has M high-priority devices, denoted by $A_m, 1 \leq m \leq M$ and cluster B has N low-priority devices, denoted by $B_n, 1 \leq n \leq N$. These IDs can harvest energy from the PB denoted P, and then use this energy to offload tasks on the UAV, denoted U, where U is equipped with a MEC server. All devices are equipped with single-antenna and operate in half-duplex mode. The Rayleigh distribution is used to characterize the small-scale fading of the channel coefficient from $a \rightarrow b, ab \in \{UA_m, UB_n, PA_m, PB_n\}$, denoted by g_{ab}, i.e., the channel power gain $|g_{ab}|^2$, is a

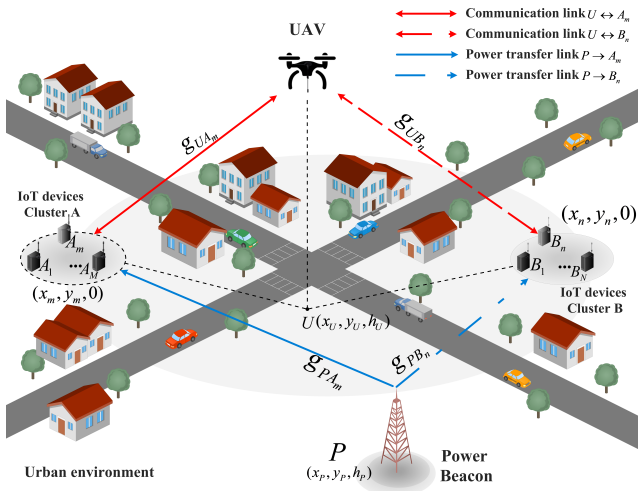

Fig. 1. System model for the UAV-aided NOMA-based WPT-MEC in IoT networks.

random variable (RV) that follows an exponential distribution with an average channel gain of λ_{ab}. Thus, the cumulative distribution function (CDF) and probability density function (PDF) of $|g_{ab}|^2$ are respectively expressed as:

$$F_{|g_{ab}|^2}(x) = 1 - e^{-\frac{x}{\lambda_{ab}}}, \tag{1}$$

$$f_{|g_{ab}|^2}(x) = \frac{1}{\lambda_{ab}} e^{-\frac{x}{\lambda_{ab}}}. \tag{2}$$

The IDs are assumed to be executing the same application with a task length of l (bits), where the tasks are independent of one another and divided into discrete groups [7]. Accordingly, the offloaded capacity of A_m and B_n is expressed as $L_I^{off} = \beta_I l$, where $I \in (A_m, B_n)$, $0 \leq \beta \leq 1$. Without loss of generality, we use a 3D Cartesian coordinate system where A_m, B_n and P are on the ground with coordinates $A_m\,(x_m, y_m, 0)$, $B_n\,(x_n, y_n, 0)$ and $P(x_P, y_P, h_P)$, respectively. The U is fixed at $h_U > 0$ [10] with coordinates $U(x_U, y_U, h_U)$. Taking into account the likelihood of both LoS and NLoS linkages between the U to IDs and P to IDs, the mean path loss is calculated as follows [5]:

$$\overline{\mathcal{L}}_{ab} = \mathcal{L}_{ab}^{los} P_{ab}^{los} + \mathcal{L}_{ab}^{nlos} P_{ab}^{nlos}, \tag{3}$$

where $P_{ab}^{los} = \frac{1}{1+\omega_1 \exp[-\omega_2(\theta_{ab}-\omega_1)]}$ and $P_{ab}^{nlos} = 1 - P_{ab}^{los}$ express the LoS and the NLoS likelihood; the distance from a to b is $d_{ab} = \sqrt{(x_b - x_a)^2 + (y_b - y_a)^2 + h_U^2}$; the elevation angle $\theta_{ab} = \frac{180}{\pi} \arcsin(\frac{h_U}{d_{ab}})$; ω_1 and ω_2 are parameters contingent on different environments (rural, urban, or dense urban) [9]; $\mathcal{L}_{ab}^{los} = \xi^{los} \frac{c d_{ab}{}^{\sigma}}{4\pi f_c}$ and $\mathcal{L}_{ab}^{nlos} = \xi^{nlos} \frac{c d_{ab}{}^{\sigma}}{4\pi f_c}$ are the path-loss exponent channels, where c is the speed of light, f_c is the carrier frequency, σ is the path-loss exponent and ξ^{los} and ξ^{nlos} are excessive path losses of the LoS and NLoS propagation.

In this work, After the IDs harvest energy from P, we perform the selection of the best ID of the two clusters to perform the offloading tasks to U. Therefore, the best ID is selected such that the best possible channel gain of the $U - A_m$ and $U - B_n$ link is achieved $|g_{I^*}|^2 = \max\{|g_{UI}|^2\}$,

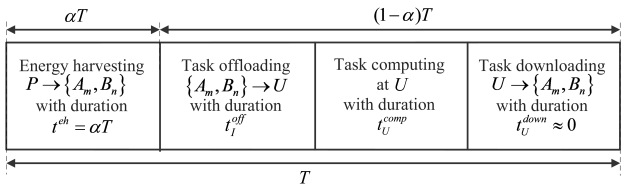

Fig. 2. Time flowchart of the considered UAV-assisted NOMA-WPT-MEC network.

where $I^* \in (A^*, B^*)$. Because the channel gains follow the Rayleigh distribution, the CDF and PDF of channel power gains $|g_{I^*}|^2$ are respectively expressed as follows:

$$F_{|g_{I^*}|^2}(x) = \sum_{t=0}^{K} \binom{K}{t} (-1)^t e^{-\frac{tx}{\lambda_x}}, \tag{4}$$

$$f_{|g_{I^*}|^2}(x) = \sum_{t=1}^{K} \binom{K}{t} \frac{(-1)^{t+1} t}{\lambda_x} e^{-\frac{tx}{\lambda_x}}, \tag{5}$$

where $K \in (M, N)$.

2.2 Communication protocol

In this subsection, we present the communication protocol for the proposed system. Fig. 2 depicts the time flow chart of the protocol. The communication protocol is detailed as follows.

- In the first phase t^{eh}, the IDs harvest energy from the P, which can be expressed as $E_{PI} = \frac{\eta P_P \alpha T |g_{PI}|^2}{\overline{\mathcal{L}}_{PI}}$, where η is the EH efficiency coefficient, $0 < \eta < 1$; P_P is transmission power of P; α is the time switching ratio (TSR), $0 < \alpha < 1$; T is the transmission block time.
- In the second phase $t_{I^*}^{off}$, the best ID in two cluster simultaneously offload $\mathcal{L}_{I^*}^{off}$ (bits) to U by using uplink NOMA. Therefore, the signal received at U is as follows:

$$y_U^{MEC} = \sqrt{\frac{P_{A^*}}{\overline{\mathcal{L}}_{UA^*}}} g_{A^*} x_{A^*} + \sqrt{\frac{P_{B^*}}{\overline{\mathcal{L}}_{UB^*}}} g_{B^*} x_{B^*} + n_U, \tag{6}$$

where x_{A^*}, x_{B^*} are the transmitted signals of the two best IDs clusters, respectively, $P_{I^*} = \frac{E_{PI^*}}{(1-\alpha)T - t_U^{comp}}$ is transmission power of I^*, and $n_U \sim \mathcal{CN}(0, N_0)$. According to the principle of uplink NOMA, U first decodes x_{A^*} after that x_{B^*} by canceling out the known x_{A^*} with [3]. Therefore, the received signal-to-interference-plus-noise ratios (SINRs) at U for detecting x_{A^*} and x_{B^*} are expressed as follows:

$$\gamma_{A^*}^U = \frac{\gamma_{A^*} \overline{\mathcal{L}}_{UB^*} SZ}{\gamma_{B^*} \overline{\mathcal{L}}_{UA^*} XY + \overline{\mathcal{L}}_{UA^*} \overline{\mathcal{L}}_{UB^*}}, \tag{7}$$

$$\gamma_{B^*}^U = \frac{\gamma_{B^*} XY}{\overline{\mathcal{L}}_{UB^*}}, \tag{8}$$

where $\gamma_P = \frac{P_p}{N_0}$, $\gamma_{A^*} = \frac{\eta \gamma_P \alpha T}{\overline{\mathcal{L}}_{PA^*}\left[(1-\alpha)T - t_U^{comp}\right]}$, $\gamma_{B^*} = \frac{\eta \gamma_P \alpha T}{\overline{\mathcal{L}}_{PB^*}\left[(1-\alpha)T - t_U^{comp}\right]}$, $X = |g_{B^*}|^2$, $Y = |g_{PB^*}|^2$, $S = |g_{A^*}|^2$, and $Z = |g_{PA^*}|^2$.

- In the third phase t_U^{comp}, the tasks that were offloaded are computed at U. Therefore, the time required to complete the total number of task bits at U can be expressed as: $t_U^{comp} =$

$\frac{\left(Ł_{A^*}^{off}+Ł_{B^*}^{off}\right)\mathbb{C}}{f_U^{mec}}$, where $\mathbb{C}$ is the number of CPU cycles requires to calculate one task bit; f_U^{mec} is the hosting frequency of the MEC sever at U.

- In the forth phase t_U^{down}, U sends back the processed results to devices in A^* and B^*. Due to the highly short delay-time and minor energy required for sending back the results, we considered t_U^{down} is approximately equals to 0 [12].

3 PERFORMANCE ANALYSIS

3.1 Successful Computation Probability

In this subsection, we proposed SCP as the probability that all offloaded task bits can be computed successfully within the time delay of the system T^{th}. The SCP is calculated as follows:

$$\Psi = \Pr\left\{\max\left(t_{A^*}^{off}, t_{B^*}^{off}\right) < T^{th}\right\}, \tag{9}$$

where $T^{th} = (1-\alpha)T - t_U^{comp}$, $t_{I^*}^{off} = \frac{L_{I^*}^{off}}{C_{I^*}}$; $C_{I^*} = WT^{th}\log_2\left(1+\gamma_{I^*}^{U}\right)$ is the channel capacity of the best ID in two cluster, and W is the bandwidth.

Lemma 3.1. *The closed-form expression of the SCP for the whole system UAV-aided NOMA-based WPT-MEC under Rayleigh fading channel is given by:*

$$\begin{aligned}\Psi = \sum_{t=1}^{M}\binom{M}{t}\frac{(-1)^{t+1}t}{\lambda_{B^*}\lambda_{PA^*}\lambda_{PB^*}}\Bigg[&\frac{2\lambda_{B^*}\lambda_{PA^*}}{t}\left(\frac{a_4 t\lambda_{PB^*}}{\lambda_{B^*}}\right)^{1/2}\mathcal{K}_1\left(2\sqrt{\frac{a_4 t}{\lambda_{B^*}\lambda_{PB^*}}}\right)\\ &-\frac{\pi^2}{4QO}\sum_{k=0}^{N}\sum_{q=1}^{Q}\sum_{o=1}^{O}\binom{N}{k}\frac{(-1)^k\sqrt{1-{\zeta_q}^2}\sqrt{1-{\zeta_o}^2}}{\omega_q\omega_o\ln^2(\omega_q)\ln^2(\omega_o)}\left(\frac{ka_1\varphi_q}{\lambda_{A^*}a_3\varphi_o}+\frac{t}{\lambda_{B^*}}\right)^{-1}\\ &\times\omega_q^{\frac{ta_4}{\lambda_{B^*}}}\omega_o^{-\frac{k(a_2+a_1a_4)}{\lambda_{A^*}a_3}}e^{-\frac{\varphi_o}{\lambda_{PA^*}}-\frac{\varphi_q}{\lambda_{PB^*}}}\Bigg],\end{aligned} \tag{10}$$

where $\theta_{A^*} = 2^{\frac{L_{A^*}^{off}}{(T^{th})^2 W}} - 1$, $\theta_{B^*} = 2^{\frac{L_{B^*}^{off}}{(T^{th})^2 W}} - 1$, $a_1 = \theta_{A^*}\gamma_{B^*}\overline{\mathcal{L}}_{UA^*}$, $a_2 = \theta_{A^*}\overline{\mathcal{L}}_{UA^*}\overline{\mathcal{L}}_{UB^*}$, $a_3 = \gamma_{A^*}\overline{\mathcal{L}}_{UB^*}$, $a_4 = \frac{\theta_{B^*}\overline{\mathcal{L}}_{UB^*}}{\gamma_{B^*}}$, *and* $\mathcal{K}_1()$ *is Bessel functions [2];* $\zeta_q = \cos\left(\frac{\pi(2q-1)}{2Q}\right)$, $\omega_q = \frac{\zeta_q+1}{2}$, $\varphi_q = -\frac{1}{\ln(\omega_q)}$, $\zeta_o = \cos\left(\frac{\pi(2o-1)}{2O}\right)$, $\omega_o = \frac{\zeta_q+1}{2}$, $\varphi_o = -\frac{1}{\ln(\omega_o)}$ *with* Q *and* O *are the complexity versus accuracy trade-off coefficient [4].*

Proof. See Appendix A. □

3.2 Problem and solution

To improve the system performance, we focused on improving the computation performance of the system by determining the optimal height of the UAV, which are denoted by h_U and the TSR, which is denoted by α^*. The SCP maximization (SCPM) problem can be expressed as

$$\begin{aligned}\underset{h_U,\,\alpha}{\text{maximize}}\quad & \Psi\\ \text{subject to}\quad & 0 \le \alpha \le 1, && \text{(11a)}\\ & 0 \le h_U \le h_U^{\max}, && \text{(11b)}\end{aligned}$$

where the conditions of TSR and the UAV height is described in constraints (11a) and (11b). The step-by-step pseudocode of PSO is given in **Algorithm 1.**

Algorithm 1 SCPM-PSO

Initialize values for parameters: ∂, μ_1, μ_2, Q, $Iter_{max}$;
Set random values for the particle positions and velocity $\mathcal{X}_i$, $\mathcal{V}_i$;
Initialize the local and global best positions: $\mathcal{P}_i$, $\mathcal{S}_i$;
For loop q to $Iter_{max}$ until the condition is met
for each particle $i = 1$ to Q **do**
    Select random numbers for r_1, r_2 values between [0,1]
    Update new position using $\mathcal{X}_i^{q+1} = \mathcal{X}_i^q + \mathcal{V}_i^{q+1}$
    Update new velocity using $\mathcal{V}_i^{q+1} = \partial \mathcal{V}_i^q + \mu_1 r_1 \left(\mathcal{P}_i^q - \mathcal{X}_i^q\right) + \mu_2 r_2 \left(\mathcal{S}_i^q - \mathcal{X}_i^q\right)$
    Update the best personal position:
    if $f(\mathcal{X}_{i+1}^q) \geq \mathcal{P}_i^q$ **then**
        $\mathcal{P}_{i+1}^q = \mathcal{X}_{i+1}^q$
    end if
    if $f(\mathcal{X}_{i+1}^q) < \mathcal{P}_i^q$ **then**
        $\mathcal{P}_{i+1}^q = \mathcal{P}_i^q$
    end if
    Update the best global position:
    $\mathcal{S}_i^q = \max(\mathcal{P}_i^q)$
    if $f(\mathcal{X}_i^q) \geq \mathcal{S}_i^q$ **then**
        $\mathcal{S}_i^q = \mathcal{X}_i^q$
    end if
    $q \leftarrow q + 1$
end for
Return: $f(\mathcal{S}_i^q)$ is the maximum value of SCP

4 NUMERICAL RESULT

In this section, we present the simulation results that verified our analysis of the SCP for UAV-aided NOMA-MEC in IoT networks over Rayleigh fading channels. The values for all system parameters of the simulations is specified in the following: $x_U = 0$, $y_U = 0$, $h_U \in (10, 50)$; $A(35, 35, 0)$; $B(20, 20, 0)$; $P(40, 40, 10)$, $\omega_1 = 0.1581$, $\omega_2 = 9.6177$; $\xi^{los} = 1$, $\xi^{nlos} = 20$; $c = 3.10^8$; $f_c = 10^5$ (Hz); $W = 10^6$(Hz); $\gamma_P \in (10, 40)$; $\alpha \in (0, 1)$; $\eta = 0.85$; $T = 1$ (s); $\theta = 2$; $l = 10^4$; $\beta_{m^*} = 0.2$, $\beta_{n^*} = 0.8$; $f_U = 10^8$ (Hz); $\mathbb{C} = 100$; $Z = 10^2$.

Fig. 3 illustrates the effect of signal-to-noise ratio (SNR) transmission γ_P and the number of IDs, M and N, on the SCP of the whole system. The simulated point closely resemble the analytical curves, demonstrating the precision of the derived expressions. In addition, the result indicates that increasing the transmit power γ_P improves of the outcome of SCP as the IDs gain more energy for the efficient offloading process then. Furthermore, the result shows that as the number of IoT devices (IDs) increases, the system'SCP improves. The more IDs exist, the more opportunities for selecting the best device in each cluster, which improves the achievable decoding performance.

Fig. 4a depicts the effect of time switching (TS) ratio on SCP of the whole system. The results forms a parabolic curve with the highest point corresponding to the TSR, α^* that maximizes SCP outcome. The reason can be explained that increasing TS ratio allows IDs to spend more time on harvesting energy but reduce time spending for the offloading duties. On the contrary, limiting TS ratio leads to the lack of energy to maintain the stability of the offloading process in the IDs. Therefore, it always exists a value α^* at which the SCP obtains its desirable value.

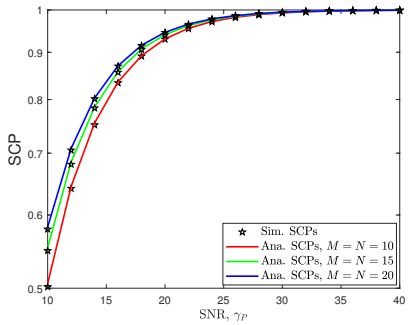

Fig. 3. The impact of SNR, γ_P on SCP of the whole system with a different M, N.

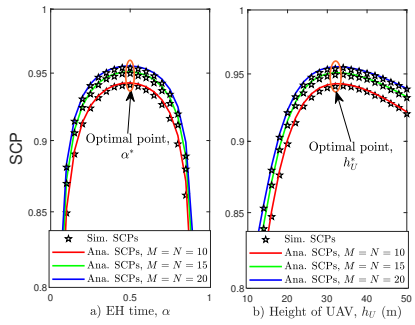

Fig. 4. The impact of TSR, α in (a) and height of UAV h_U in (b) on SCP of the whole system

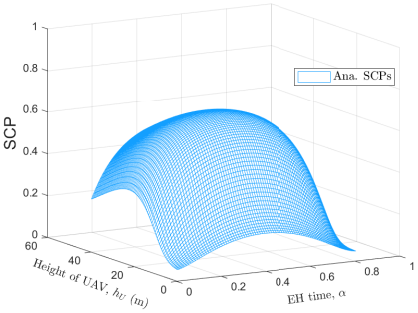

Fig. 5. The impact of both EH time and height of UAV on SCP of the whole system.

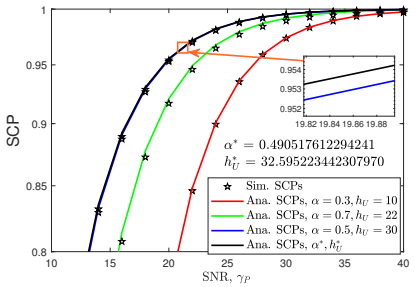

Fig. 6. The impact of optimal UAV's height and EH time on SCP of the whole system.

Fig. 4b shows the impact of the UAV height on SCP of the whole system. We can see, it appears that there is always an optimum h_U value for which the SCP value is maximum. When the height of UAV is low, the LoS probability is low, while the NLoS probability is high, that keeps the SCP value low. Increasing the h_U value can solve the problem; however, the higher the UAV is, the greater distances from it to the IDs are, which cause the waste of more transmission power. As a consequence, there is a point at which the optimum SCP is reached corresponding to the height of the UAV ${h_U}^*$.

After simultaneously running the results in Fig. 4a and Fig. 4b, we have generated a 3D simulation, illustrated by Fig. 5, considering both α and h_U on SCP of the whole system. Similar to the explanation in Figs. 4a and 4b, we can see that there is always an optimal α value and the maximum height of UAV that can maximize the SCP's value. We calculated these values by applying the PSO algorithm, introduced in **Algorithm 1**.

In Fig. 6, we compare the SCP performance at the desirable point, given on the simulation, with different fixed values of UAV's height and TS ratio. We can see that the optimal h_U^* and α^* return the best value for the SCPs.

5 CONCLUSION

In this paper, we investigated the performance of a UAV-aided NOMA-based WPT-MEC in IoT networks over a Rayleigh fading channel. We proposed a protocol to perform EH and offloading tasks. To evaluate offloading performance, a closed-form expression of SCP was derived for the whole system. In addition, in order to improve the efficiency of offloading tasks, we proposed a problem to optimize the EH time of the ID and the height of the UAV to maximize the SCP. The problem is solved based on the PSO algorithm. We provided numerical results to verify the proposed system's offloading performance.

A PROOF OF LEMMA 3.1

From (9), we can rewrite the Ψ for the whole system as

$$\begin{aligned}\Psi &= \Pr\left\{S > \frac{a_1XY + a_2}{a_3Z}, X > \frac{a_4}{Y}\right\} \\ &= \underbrace{\int_0^\infty \int_0^\infty \underbrace{\int_{\frac{a_4}{Y}}^\infty \left[1 - F_S\left(\frac{a_1XY + a_2}{a_3Z}\right)\right] f_X(x)\, dX\, f_Y(y)\, dY}_{I_1} f_Z(z)\, dZ}_{I_2},\end{aligned} \tag{12}$$

where $\theta_{A^*} = 2^{\frac{L_{A^*}^{off}}{(T^{th})^2 W}} - 1$, $\theta_{B^*} = 2^{\frac{L_{B^*}^{off}}{(T^{th})^2 W}} - 1$, $a_1 = \theta_{A^*}\gamma_{B^*}\overline{\mathcal{L}}_{UA^*}$, $a_2 = \theta_{A^*}\overline{\mathcal{L}}_{UA^*}\overline{\mathcal{L}}_{UB^*}$, $a_3 = \gamma_{A^*}\overline{\mathcal{L}}_{UB^*}$, and $a_4 = \frac{\theta_{B^*}\overline{\mathcal{L}}_{UB^*}}{\gamma_{B^*}}$. By substituting the CDF in (4) and the PDF in (5) into (10), the I_1 can be rewritten as:

$$\begin{aligned}I_1 &= \sum_{t=1}^{M}\binom{M}{t}\frac{(-1)^{t+1}t}{\lambda_{B^*}}\left[\int_{\frac{a_4}{Y}}^\infty e^{-\frac{tX}{\lambda_{B^*}}}dX - \sum_{k=0}^{N}\binom{N}{k}(-1)^k \int_{\frac{a_4}{Y}}^\infty e^{-\frac{k(a_1XY+a_2)}{\lambda_{A^*}a_3Z} - \frac{tX}{\lambda_{B^*}}}dX\right] \\ &= \sum_{t=1}^{M}\binom{M}{t}\frac{(-1)^{t+1}t}{\lambda_{B^*}}\left[\frac{\lambda_{B^*}}{t}e^{-\frac{a_4t}{\lambda_{B^*}Y}} - \sum_{k=0}^{N}\binom{N}{k}(-1)^k \right. \\ &\qquad \left. \times\left(\frac{ka_1Y}{\lambda_{A^*}a_3Z} + \frac{t}{\lambda_{B^*}}\right)^{-1} e^{-\frac{ka_2}{\lambda_{A^*}a_3Z} - \left(\frac{ka_1Y}{\lambda_{A^*}a_3Z} + \frac{t}{\lambda_{B^*}}\right)\frac{a_4}{Y}}\right].\end{aligned} \tag{13}$$

The integrals of I_1 are solved by applying the Eq. $(3.351.2^{11})$ in [2] shown in (13). Next, we substitute I_1 and the PDF in (2) into integral I_2, which can be expressed as follows:

$$\begin{aligned}I_2 &= \sum_{t=1}^{M}\binom{M}{t}\frac{(-1)^{t+1}t}{\lambda_{B^*}\lambda_{PB^*}}\left[\int_0^\infty \frac{\lambda_{B^*}}{t}e^{-\frac{a_4t}{\lambda_{B^*}Y} - \frac{Y}{\lambda_{PB^*}}}dY - \sum_{k=0}^{N}\binom{N}{k}(-1)^k \right. \\ &\qquad \left. \times\int_0^\infty \left(\frac{ka_1Y}{\lambda_{A^*}a_3Z} + \frac{t}{\lambda_{B^*}}\right)^{-1} e^{-\frac{ka_2}{\lambda_{A^*}a_3Z} - \left(\frac{ka_1Y}{\lambda_{A^*}a_3Z} + \frac{t}{\lambda_{B^*}}\right)\frac{a_4}{Y} - \frac{Y}{\lambda_{PB^*}}}dY\right].\end{aligned} \tag{14}$$

From (14), we solve the first integral of I_2 by applying Eq. 3.471.9 in [2] and the second integral by the Gaussian-Chebyshev quadrature method [4], the I_2 an be rewritten as:

$$I_2 = \sum_{t=1}^{M} \binom{M}{t} \frac{(-1)^{t+1} t}{\lambda_{B^*} \lambda_{PB^*}} \left[\frac{2\lambda_{B^*}}{t} \left(\frac{a_4 t \lambda_{PB^*}}{\lambda_{B^*}} \right)^{1/2} \mathcal{K}_1 \left(2\sqrt{\frac{a_4 t}{\lambda_{B^*} \lambda_{PB^*}}} \right) \right.$$
$$\left. - \frac{\pi}{2Q} \sum_{k=0}^{N} \sum_{q=1}^{Q} \binom{N}{k} \frac{(-1)^k \sqrt{1-\zeta_q^2}}{\omega_q \ln^2(\omega_q)} \left(\frac{k a_1 \varphi_q}{\lambda_{A^*} a_3 Z} + \frac{t}{\lambda_{B^*}} \right)^{-1} \omega_q^{\frac{t a_4}{\lambda_{B^*}}} e^{-\frac{k(a_2 + a_1 a_4)}{\lambda_{A^*} a_3 Z} - \frac{\varphi_q}{\lambda_{PB^*}}} \right], \tag{15}$$

where $\mathcal{K}_1()$ is Bessel functions; $\zeta_q = \cos\left(\frac{\pi(2q-1)}{2Q}\right)$, $\omega_q = \frac{\zeta_q + 1}{2}$, $\varphi_q = -\frac{1}{\ln(\omega_q)}$, with Q is the complexity versus accuracy trade-off coefficient. After that, we substitute (15) and the PDF in (2) into integral in (12). The Ψ can be expressed as:

$$\Psi = \sum_{t=1}^{M} \binom{M}{t} \frac{(-1)^{t+1} t}{\lambda_{B^*} \lambda_{PA^*} \lambda_{PB^*}} \left[\frac{2\lambda_{B^*}}{t} \left(\frac{a_4 t \lambda_{PB^*}}{\lambda_{B^*}} \right)^{1/2} \mathcal{K}_1 \left(2\sqrt{\frac{a_4 t}{\lambda_{B^*} \lambda_{PB^*}}} \right) \right.$$
$$\times \int_0^{\infty} e^{-\frac{Z}{\lambda_{PA^*}}} dZ - \frac{\pi}{2Q} \sum_{k=0}^{N} \sum_{q=1}^{Q} \binom{N}{k} \frac{(-1)^k \sqrt{1-\zeta_q^2}}{\omega_q \ln^2(\omega_q)} \omega_q^{\frac{t a_4}{\lambda_{B^*}}} e^{-\frac{\varphi_q}{\lambda_{PB^*}}}$$
$$\left. \times \int_0^{\infty} \left(\frac{k a_1 \varphi_q}{\lambda_{A^*} a_3 Z} + \frac{t}{\lambda_{B^*}} \right)^{-1} e^{-\frac{k(a_2 + a_1 a_4)}{\lambda_{A^*} a_3 Z} - \frac{Z}{\lambda_{PA^*}}} dZ \right]. \tag{16}$$

Similar to (14), we solve the first integral of Ψ by applying Eq. 3.310[11] in [2] and the second integral by again the Gaussian-Chebyshev quadrature method [4], the Ψ an be rewritten as:

$$\Psi = \sum_{t=1}^{M} \binom{M}{t} \frac{(-1)^{t+1} t}{\lambda_{B^*} \lambda_{PA^*} \lambda_{PB^*}} \left[\frac{2\lambda_{B^*} \lambda_{PA^*}}{t} \left(\frac{a_4 t \lambda_{PB^*}}{\lambda_{B^*}} \right)^{1/2} \mathcal{K}_1 \left(2\sqrt{\frac{a_4 t}{\lambda_{B^*} \lambda_{PB^*}}} \right) \right.$$
$$- \frac{\pi^2}{4QO} \sum_{k=0}^{N} \sum_{q=1}^{Q} \sum_{o=1}^{O} \binom{N}{k} \frac{(-1)^k \sqrt{1-\zeta_q^2} \sqrt{1-\zeta_o^2}}{\omega_q \omega_o \ln^2(\omega_q) \ln^2(\omega_o)} \left(\frac{k a_1 \varphi_q}{\lambda_{A^*} a_3 \varphi_o} + \frac{t}{\lambda_{B^*}} \right)^{-1}$$
$$\left. \times \omega_q^{\frac{t a_4}{\lambda_{B^*}}} \omega_o^{-\frac{k(a_2 + a_1 a_4)}{\lambda_{A^*} a_3}} e^{-\frac{\varphi_o}{\lambda_{PA^*}} - \frac{\varphi_q}{\lambda_{PB^*}}} \right], \tag{17}$$

where $\zeta_o = \cos\left(\frac{\pi(2o-1)}{2O}\right)$, $\omega_o = \frac{\zeta_q + 1}{2}$, $\varphi_o = -\frac{1}{\ln(\omega_o)}$, and O is the complexity versus accuracy trade-off coefficient of the Gaussian-Chebyshev quadrature. This ends our proof.

REFERENCES

[1] Saad El Jaouhari and Eric Bouvet. 2022. Secure firmware Over-The-Air updates for IoT: Survey, challenges, and discussions. *Internet of Things* 18 (2022), 100508. https://doi.org/10.1016/j.iot.2022.100508

[2] I.S. Gradshteyn and I.M. Ryzhik. 2014. *Table of Integrals, Series, and Products.* USA: Academic Press.

[3] Zoran Hadzi-Velkov, Slavche Pejoski, Nikola Zlatanov, and Robert Schober. 2020. UAV-Assisted Wireless Powered Relay Networks With Cyclical NOMA-TDMA. *IEEE Wireless Commun. Lett.* 9, 12 (Dec. 2020), 2088–2092.

[4] K. L. Judd. 2012. Quadrature Methods presented at University of Chicago's Initiative for Computational Economics.

[5] Anh-Nhat Nguyen and Ngoc-Anh Bui. 2023. Performance Analysis of IoT Mobile Edge Computing Networks Using a DF/AF UAV-Enabled Relay with Downlink NOMA. In *Proc. ISIEA, Kuala Lumpur, Malaysia.* 1–6.

[6] Anh-Nhat Nguyen, Dac-Binh Ha, Van-Truong Truong, Van Nhan Vo, Surasak Sanguanpong, and Chakchai So-In. 2023. Secrecy Performance Analysis and Optimization for UAV-Relay-Enabled WPT and Cooperative NOMA MEC in IoT Networks. *IEEE Access* (2023), 1–1.

[7] A. N. Nguyen, D. B. Ha, V. N. Vo, V. T. Truong, D. T. Do, and C. So-In. 2022. Performance Analysis and Optimization for IoT Mobile Edge Computing Networks With RF Energy Harvesting and UAV Relaying. *IEEE Access* 23, 10 (Feb. 2022), 21526 – 21540.

[8] Anh-Nhat Nguyen, Van Nhan Vo, C. So-In, and D. Ha. 2021. System Performance Analysis for an Energy Harvesting IoT System Using a DF/AF UAV-Enabled Relay with Downlink NOMA under Nakagami-*m* Fading. *Sensors* 21, 1 (Jan. 2021).

[9] Anh-Nhat Nguyen, Van Nhan Vo, C. So-In, D. Ha, and Van-Truong Truong. 2021. Performance Analysis in UAV-enabled Relay with NOMA under Nakagami-*m* Fading Considering Adaptive Power Splitting. In *Proc. JCSSE, Lampang, Thailand.* 1–6.

[10] W. Mei Q. Wang, Z. Chen and J. Fang. 2017. Improving physical layer security using UAV-enabled mobile relaying. *IEEE Trans. Wireless Commun.* 6, 3 (Jun 2017), 310–313.

[11] V. T. Truong, D. B. Ha, Y. Lee, and A. N. Nguyen. 2020. On Performance of Cooperative Transmission in Uplink Non-Orthogonal Multiple Access Wireless Sensor Networks. *International Conference on Recent Advances in Signal Processing, Telecommunications and Computing (SigTelCom)* (Sep. 2020), 56–60.

[12] T. Zhang, Y. Xu, J. Loo, D. Yang, and L. Xiao. 2020. Joint Computation and Communication Design for UAV-Assisted Mobile Edge Computing in IoT. *IEEE Trans. on Indus.* 16, 8 (Aug. 2020), 5505 – 5516.

[13] Z. Zhang, H. Pang, A. Georgiadis, and C. Cecati. 2018. Wireless Power Transfer – An Overview. *IEEE Trans. on Indust.* 66 (Feb. 2018), 1044 – 1058.

[14] F. Zhou, Y. Wu, R. Qingyang Hu, and Y. Qian. 2018. Computation Rate Maximization in UAV-Enabled Wireless-Powered Mobile-Edge Computing Systems. *IEEE Jour. on Selec.* 36, 9 (Sep. 2018), 1927 – 1941.